Spin crossover in $(Mg,Fe^{3+})(Si,Fe^{3+})O_3$ bridgmanite: effects of disorder, iron concentration, and temperature

Gaurav Shukla[a,*], Renata M. Wentzcovitch[a,b]

[a]*School of Physics and Astronomy, University of Minnesota, Minneapolis, Minnesota, USA*
[b]*Department of Chemical Engineering and Materials Science, University of Minnesota, Minneapolis, Minnesota, USA*

Abstract

The spin crossover of iron in Fe^{3+}-bearing bridgmanite, the most abundant mineral of the Earths lower mantle, is by now a well-established phenomenon, though several aspects of this crossover remain unclear. Here we investigate effects of disorder, iron concentration, and temperature on this crossover using *ab initio* LDA + U_{sc} calculations. The effect of concentration and disorder are addressed using complete statistical samplings of coupled substituted configurations in super-cells containing up to 80 atoms. Vibrational/thermal effects on the crossover are addressed within the quasiharmonic approximation. The effect of disorder seems quite small, while increasing iron concentration results in considerable increase in crossover pressure. Our calculated compression curves for iron-free, Fe^{2+}-, and Fe^{3+}-bearing bridgmanite compare well with the latest experimental measurements. The comparison also suggests that in a close system, Fe^{2+} present in the sample may transform into Fe^{3+} by introduction of Mg and O vacancies with increasing pressure. As in the spin crossover in ferropericlase, this crossover in bridgmanite is accompanied by a clear volume reduction and an anomalous softening of the bulk modulus throughout the crossover pressure range. These effects reduce significantly with increasing temperature. Though the concentration of $[Fe^{3+}]_{Si}$ in bridgmanite may be small, related elastic anomalies may impact the interpretation of radial and lateral velocity structures of the Earth's lower mantle.

Keywords: Bridgmanite, Lower mantle, Spin crossover, Thermoelasticity

1. Introduction

Bridgmanite (br), $(Mg,Fe,Al)(Si,Fe,Al)O_3$ perovskite (Pv), is the main constituent of the Earth's lower mantle along with $(Mg,Fe)O$, $CaSiO_3$ Pv, and $(Mg,Fe,Al)(Si,Fe,Al)O_3$ post-perovskite (PPv). Thermodynamics and elastic properties of these minerals provide a direct link to seismic tomographic models. Understanding the effect of iron (Fe) and/or aluminum (Al) sub-

*Corresponding author
Email addresses: shuk0053@umn.edu (Gaurav Shukla), wentz002@umn.edu (Renata M. Wentzcovitch)

stitutions on the physical, chemical, and thermodynamic properties of the host mineral is essential to constrain the composition and thermal structure of the Earth's lower mantle. Ferropericlase (Fp), (Mg,Fe)O, is known to undergo a pressure induced spin crossover from the high (S=2) to the low-spin (S=0) state, which affects its elastic and thermal properties (*Badro et al.*, 2003; *Goncharov et al.*, 2006; *Tsuchiya et al.*, 2006; *Fei et al.*, 2007; *Crowhurst et al.*, 2008; *Marquardt et al.*, 2009; *Wu et al.*, 2009; *Wentzcovitch et al.*, 2009; *Antonangeli et al.*, 2011; *Mao et al.*, 2011; *Wu et al.*, 2013; *Hsu and Wentzcovitch*, 2014; *Wu and Wentzcovitch*, 2014).

In the case of iron-bearing bridgmanite, in spite of considerable progress of experimental measurements at high pressures and high temperatures (*Badro et al.*, 2004; *Li et al.*, 2004; *Jackson et al.*, 2005a; *Li et al.*, 2006; *Lin et al.*, 2008; *Lundin et al.*, 2008; *McCammon et al.*, 2008; *Dubrovinsky et al.*, 2010; *McCammon et al.*, 2010; *Boffa Ballaran et al.*, 2012; *Chantel et al.*, 2012; *Fujino et al.*, 2012; *Hummer and Fei*, 2012; *Lin et al.*, 2012; *Dorfman et al.*, 2013; *Lin et al.*, 2013; *McCammon et al.*, 2013; *Sinmyo et al.*, 2014; *Mao et al.*, 2015), deciphering the valence and spin states of multivalent iron and its influence on the physical properties has been quite a formidable challenge due to complexity of the perovskite structure. Iron in bridgmanite may exists in ferrous (Fe^{2+}) and ferric (Fe^{3+}) states. Fe^{2+} occupies the A-site ($[Fe^{2+}]_{Mg}$), while Fe^{3+} can occupy A- ($[Fe^{3+}]_{Mg}$) and/or B-site ($[Fe^{3+}]_{Si}$) of the perovskite structure (*Badro et al.*, 2004; *Li et al.*, 2004; *Jackson et al.*, 2005a; *Li et al.*, 2006; *Stackhouse et al.*, 2007; *Bengtson et al.*, 2009; *Lin et al.*, 2008; *Dubrovinsky et al.*, 2010; *Hsu et al.*, 2010, 2011; *Fujino et al.*, 2012; *Hummer and Fei*, 2012; *Lin et al.*, 2012, 2013; *Tsuchiya and Wang*, 2013; *Sinmyo et al.*, 2014; *Mao et al.*, 2015). In the entire lower mantle pressure-range, $[Fe^{2+}]_{Mg}$ remains in the HS state (S=2) but undergoes a pressure induced lateral displacement resulting in the state with increased iron Mössbauer quadrupole splitting (QS) (*McCammon et al.*, 2008; *Bengtson et al.*, 2009; *Hsu et al.*, 2010; *Lin et al.*, 2012, 2013; *McCammon et al.*, 2013; *Potapkin et al.*, 2013; *Kupenko et al.*, 2014; *Shukla et al.*, 2015a,b). By contrast, $[Fe^{3+}]_{Si}$ undergoes a crossover from HS (S=5/2) to LS (S=1/2) state, while $[Fe^{3+}]_{Mg}$ remains in the HS (S=5/2) state (*Catalli et al.*, 2010; *Hsu et al.*, 2011; *Lin et al.*, 2012, 2013; *Tsuchiya and Wang*, 2013; *Mao et al.*, 2015; *Xu et al.*, 2015).

The onset of the HS to LS crossover of $[Fe^{3+}]_{Si}$ in Fe^{3+}-bearing bridgmanite (Fe^{3+}-br) is still much debated. For Fe^{3+}-br with 10 mol.% Fe_2O_3, *Catalli et al.* (2010) observed the crossover completion at 48 GPa by X-ray emission spectroscopy(XES), and a change in electronic configuration between 53 and 63 GPa by Synchrotron Mössbauer spectroscopy (SMS). These observations led them to conclude the crossover pressure range to be approximately 48-63 GPa. Using SMS, *Lin et al.* (2012) found the crossover pressure range 13-24 GPa for a sample containing about ~2.0-2.5% of Fe^{3+}. *Lin et al.* (2012) and *Mao et al.* (2015) further argued that the lower crossover pressure observed by them could be related to the smaller Fe^{3+} concentration in their samples. Using first-principles static LDA + U$_{sc}$ and GGA + U$_{sc}$ calculations for $(Mg_{1-x}Fe^{3+}_x)(Si_{1-x}Fe^{3+}_x)O_3$ with $x = 0.125$, *Hsu et al.* (2011) estimated the crossover pressure 41 GPa and 70 GPa, respectively, while *Tsuchiya and Wang* (2013) reported 44 GPa for $x = 0.0625$ using LDA + U calculations. A thermodynamic model by *Xu et al.* (2015) estimated the $Fe^{3+}/\sum Fe$ ratio

under lower mantle conditions to be ~0.01-0.07 in Al-free bridgmanite. In an effort to understand and reconcile observations and results of these studies, we have investigated the effect of 1) disordered substitution of nearest neighbor Fe^{3+}-Fe^{3+} pairs, 2) Fe^{3+} concentration, and 3) vibrational effects on the HS to LS crossover in Fe^{3+}-bearing bridgmanite.

2. Computational details and Methodology

2.1. Computational details

Density functional theory (DFT) within the local density approximation (LDA) (*Ceperley and Alder*, 1980) has been used in this study. It is well known that standard DFT functionals do not capture strong correlation effects of $3d$ and $4f$ electrons properly. For this reason, standard DFT is augmented by the the self- and structurally consistent Hubbard U_{sc} (LDA + U_{sc} method) (*Cococcioni and de Gironcoli*, 2005; *Kulik et al.*, 2006; *Hsu et al.*, 2009). U_{sc} values reported by *Hsu et al.* (2011) using these methods have been used here. Disordered substitution of Fe^{3+} in $(Mg_{1-x}Fe_x^{3+})(Si_{1-x}Fe_x^{3+})O_3$ bridgmanite with varying iron concentration has been investigated in 80- (x = 0.125), 40- (x = 0.25), and 20-atoms (x = 0.50) super-cells (Fig. 1). Ultrasoft pseudo-potentials (*Vanderbilt*, 1990) have been used for Fe, Si, and O. For Mg, a norm-conserving pseudo-potential, generated by von Barth-Car's method, has been used. A detailed description of these pseudo-potentials has been reported by *Umemoto et al.* (2008). The plane-wave kinetic energy and charge density cut-off are 40 Ry and 160 Ry, respectively. For 80-, 40-, and 20-atom super-cells, the electronic states were sampled on a shifted $2 \times 2 \times 2$, $4 \times 4 \times 4$, and $6 \times 6 \times 4$ k-point grid, respectively. Structural optimization at arbitrary pressure has been performed using variable cell-shape damped molecular dynamics (*Wentzcovitch*, 1991; *Wentzcovitch et al.*, 1993). Structures are optimized until the inter-atomic forces are smaller than 10^{-4} $Ry/a.u.$ Vibrational density of states (VDOS) for Fe^{3+} concentration x = 0.125 has been calculated in a 40-atom super-cell using density functional perturbation theory (DFPT) (*Baroni et al.*, 2001) within the LDA + U_{sc} functional (*Floris et al.*, 2011). For this purpose, dynamical matrices on a $2 \times 2 \times 2$ q-point grid of a 40-atom cell were calculated and thus obtained force constants were interpolated on a $8 \times 8 \times 8$ q-point grid. High throughput calculations have been performed using the VLab cyberinfrastructure at the Minnesota Supercomputing Institute (*da Silveira et al.*, 2008).

2.2. Disordered substitution of Fe^{3+} and spin crossover

Disordered substitution of Fe^{3+} in $(Mg_{1-x}Fe_x^{3+})(Si_{1-x}Fe_x^{3+})O_3$ has been studied by replacing nearest neighbor Mg^{2+}-Si^{4+} pairs with $[Fe^{3+}]_{Mg}$-$[Fe^{3+}]_{Si}$ pairs and generating all possible atomic configurations consistent with super-cell size. The number of symmetrically inequivalent configurations, N_c, are 21, 13, and 5 in 80- (x = 0.125), 40- (x = 0.25), and 20-atom (x = 0.50) super-cells, respectively. Within the quasiharmonic approximation (QHA) (*Umemoto et al.*, 2010), the partition function for disordered system with $[Fe^{3+}]_{Si}$ in a spin state σ is given by

$$Z_\sigma^{QHA}(T,V) = \sum_{i=1}^{N_c} g_i M_\sigma \exp\left\{-\frac{E_\sigma^i(V)}{k_B T}\right\} \times \prod_{j=1}^{N_{mode}} \left[\sum_{v_{i,j}=0}^{\infty} \exp\left\{-\left(v_{i,j}+\frac{1}{2}\right)\frac{\hbar\omega_{i,j,\sigma}(V)}{k_B T}\right\}\right], \tag{1}$$

3
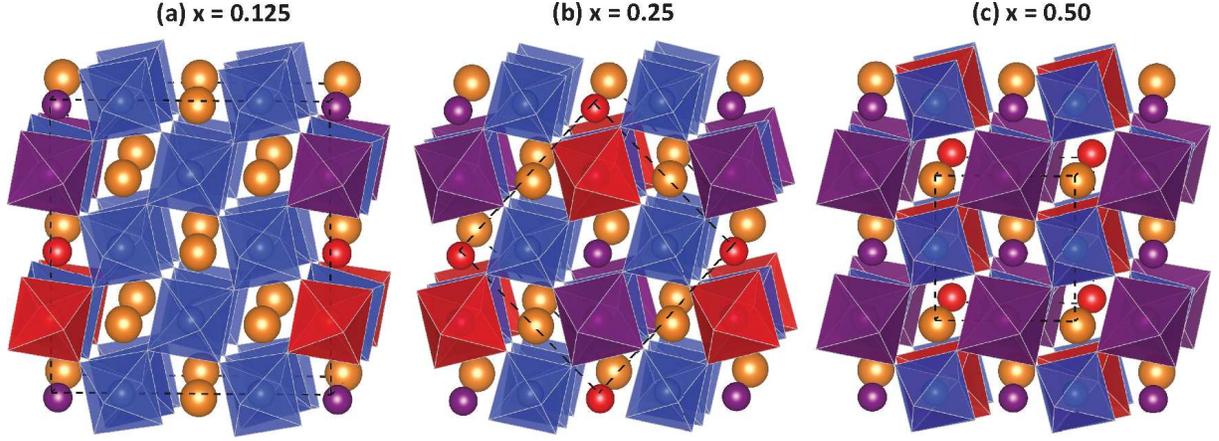
Figure 1: (Color online) Lowest enthalpy atomic configurations for two (purple and red) nearest neighbor $[Fe^{3+}]_{Mg}$-$[Fe^{3+}]_{Si}$ pairs in $(Mg_{1-x}Fe_x^{3+})(Si_{1-x}Fe_x^{3+})O_3$ bridgmanite. Unit cells consists of 80 atoms ($2 \times 2 \times 1$ super-cell) for x = 0.125, 40 atoms ($\sqrt{2} \times \sqrt{2} \times 1$ super-cell) for x = 0.25, and 20 atoms for x = 0.50 are shown by black dashed lines. There are 21, 13, and 5 configurations in 80, 40, and 20 atoms unit-cell, respectively. Si-O octahedron and Mg atom is represented by blue and orange color, respectively.

where g_i is the multiplicity of symmetrically equivalent configurations and $E_\sigma^i(V)$ is the static energy of the ith inequivalent configuration at volume V. M_σ is the magnetic degeneracy of the system, which includes the spin and orbital degeneracies. $\nu_{i,j}$ and $\omega_{i,j,\sigma}(V)$ are the number of excited phonons and frequency of jth mode at volume V for i^{th} configuration. k_B and $\hbar$ are Boltzmann and Planck constants, respectively. N_c and N_{mode} are the total number of configurations and vibrational modes of a given super-cell. After summing over $\nu_{i,j}$, the partition function is written as

$$Z_\sigma^{QHA}(T,V) \quad = \quad \sum_{i=1}^{N_c} g_i M_\sigma \exp\left\{-\frac{E_\sigma^i(V)}{k_B T}\right\} \times \prod_{j=1}^{N_{mode}} \left\{\frac{\exp\left(-\frac{\hbar\omega_{i,j,\sigma}(V)}{2k_B T}\right)}{1 - \exp\left(-\frac{\hbar\omega_{i,j,\sigma}(V)}{k_B T}\right)}\right\}. \tag{2}$$

The computation of VDOS (i.e., phonon frequencies $\omega_{i,j,\sigma}(V)$) within DFPT + U_{sc} method (*Floris et al.*, 2011) for every symmetrically inequivalent configuration is extremely challenging. To circumvent this difficulty, we approximate the partition function by assuming that VDOS for a given Fe^{3+} concentration x is same for all configurations. Within this approximation, the partition function becomes

$$Z_\sigma^{QHA}(T,V) \quad = \quad \left[\sum_{i=1}^{N_c} g_i M_\sigma \exp\left\{-\frac{E_\sigma^i(V)}{k_B T}\right\}\right] \times \left[\prod_{j=1}^{N_{mode}} \frac{\exp\left\{-\frac{\hbar\omega_{j,\sigma}(V)}{2k_B T}\right\}}{\left\{1 - \exp\left(-\frac{\hbar\omega_{j,\sigma}(V)}{k_B T}\right)\right\}}\right]. \tag{3}$$

The Helmholtz free-energy for the system (the super-cell containing N formula units of Fe^{3+}-br) with $[Fe^{3+}]_{Si}$ in HS/LS state can be calculated as

$$\begin{aligned} F_{HS/LS}(T,V) \quad &= \quad -k_B T \ln\left[Z_{HS/LS}^{QHA}(T,V)\right] \tag{4} \\ &= \quad F_{HS/LS}^{conf}(T,V) + F_{HS/LS}^{vib}(T,V) + F_{HS/LS}^{mag}(T,V), \end{aligned}$$

4

where $F_{HS/LS}^{conf}(T, V)$ is the free-energy contribution due to the statistical distribution of symmetrically inequivalent configurations and $F_{HS/LS}^{vib}(T, V)$ is the vibrational contribution. The magnetic contribution to the free-energy, $F_{HS/LS}^{mag}(T, V)$, is

$$F_{HS/LS}^{mag}(T, V) = -k_B T ln\left(M_{HS/LS}\right). \tag{5}$$

As mentioned before, Fe^{3+} in $(Mg_{1-x}Fe_x^{3+})(Si_{1-x}Fe_x^{3+})O_3$ occupies as a coupled $[Fe^{3+}]_{Mg}$-$[Fe^{3+}]_{Si}$ pair with molar fraction x, where $[Fe^{3+}]_{Mg}$ is always in the HS state while $[Fe^{3+}]_{Si}$ undergoes HS to LS crossover. Therefore, magnetic degeneracies M_{HS} and M_{LS} for a system containing N formula units of Fe^{3+}-br in a super-cell (i.e., super-cell having Nx $[Fe^{3+}]_{Mg}$-$[Fe^{3+}]_{Si}$ pairs) are given by

$$
\begin{aligned}
M_{HS} &= [m_{HS}(S_{HS} + 1) \times m_{HS}(S_{HS} + 1)]^{Nx} \quad and \\
M_{LS} &= [m_{HS}(S_{HS} + 1) \times m_{LS}(S_{LS} + 1)]^{Nx},
\end{aligned}
\tag{6}
$$

where $m_{HS/LS}$ and $S_{HS/LS}$, respectively, are the orbital degeneracy and total spin of Fe^{3+} in HS and LS state. The Gibb's free-energy of the system with $[Fe^{3+}]_{Si}$ in HS/LS state can be calculated as $G_{HS/LS}(T, V) = F_{HS/LS}(T, V) + PV$, which is then converted to $G_{HS/LS}(T, P)$.

To investigate the effect of HS to LS crossover of $[Fe^{3+}]_{Si}$, we consider the mixed state (MS) of HS and LS within the ideal solid solution approximation. This solid solution model of HS and LS iron is carried out in the $[Fe^{3+}]_{Si}$ sub-lattice only and is very appropriate for this type of problem (*Wentzcovitch et al.*, 2009; *Wu et al.*, 2009, 2013). The Gibb's free-energy per formula unit for the MS state is given by

$$G(P, T, n) = nG_{LS}(P, T) + (1 - n)G_{HS}(P, T) + G^{mix}(P, T), \tag{7}$$

where n is the low-spin fraction, and the mixing free-energy $G^{mix}(P, T)$ is

$$G^{mix}(P, T) = k_B T x[nln(n) + (1 - n)ln(1 - n)]. \tag{8}$$

Minimizing free-energy $G(P, T, n)$ (Eq. 7) with respect to LS fraction, n, we obtain

$$n(P, T) = \frac{1}{1 + \frac{m_{HS}(2S_{HS}+1)}{m_{LS}(2S_{LS}+1)} \exp\left\{\frac{\Delta G_{LS-HS}^{conf+vib}}{x k_B T}\right\}}, \tag{9}$$

where $\Delta G_{LS-HS}^{conf+vib} = G_{LS}^{conf+vib} - G_{HS}^{conf+vib}$. For $[Fe^{3+}]_{Si}$ enclosed by ordered oxygen octahedron, orbital degeneracies are m_{HS} = 1 and m_{LS} = 3. Since the degeneracies of e_g and t_{2g} in the perovskite structure (as in the case of Fe^{3+}-bearing bridgmanite) are broken due to the presence of asymmetry in oxygen octahedron, m_{LS} = 1 has been used in most of the cases. However, to assess the effect of orbital degeneracies, m_{LS} = 3 case has also been tested while addressing the vibrational effects.
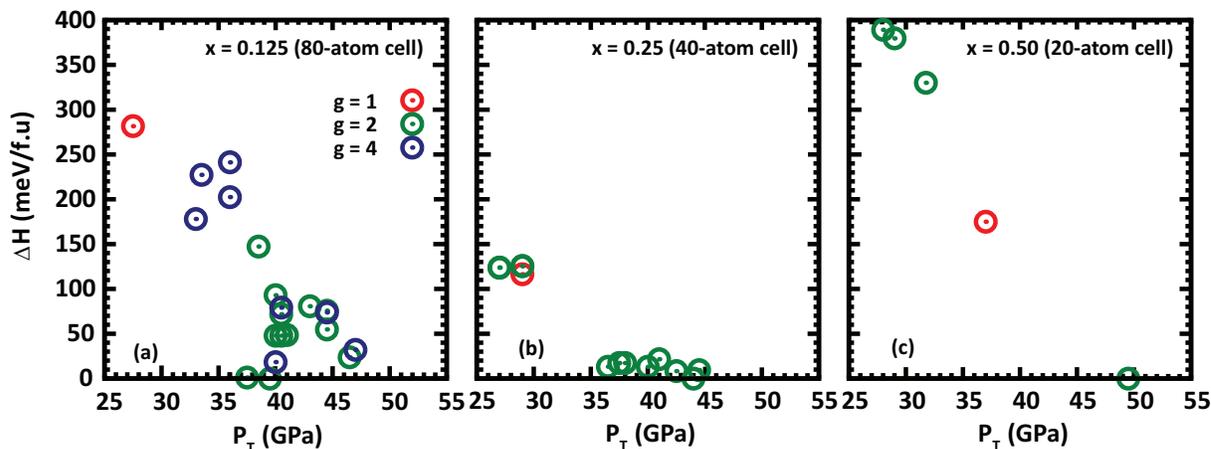
5

Figure 2: (Color online) Relative enthalpy per formula unit (f.u) at crossover pressures of all configurations with respect to lowest enthalpy configuration for (a) $x = 0.125$ (80 atoms), (b) $x = 0.25$ (40 atoms), and (c) $x = 0.50$ (20 atoms), respectively. g is multiplicity of configurations shown by red, green, and blue colors.

3. Results and discussion

3.1. Effect of disorder on spin crossover

We investigate the solid solution of $(Mg_{1-x}Fe_x)(Si_{1-x}Fe_x)O_3$ by sampling the complete phase space of configurations of $[Fe^{3+}]_{Mg}$-$[Fe^{3+}]_{Si}$ pairs in super-cells containing 80-, 40-, and 20-atoms. We consider only configurations with coupled substitution, i.e., $[Fe^{3+}]_{Mg}$-$[Fe^{3+}]_{Si}$ pairs since they are the lowest energy configurations (*Stackhouse et al.*, 2007; *Hsu et al.*, 2011). Representative crystal structures for this type of substitutions are shown in Fig. 1. Two $[Fe^{3+}]_{Mg}$-$[Fe^{3+}]_{Si}$ pairs (shown in purple and red color) are substituted in the 80, 40, and 20-atoms super-cell for x = 0.125, 0.25, and 0.50, respectively. There are 21, 13, and 5 symmetrically inequivalent configurations, respectively, in these super-cells. Static crossover pressures in $[Fe^{3+}]_{Si}$ and their relative enthalpy at crossover point for each configurations are shown in Fig. 2. Crossover pressures for these configurations are in ~27.5 GPa to ~50.0 GPa pressure range. The lowest enthalpy configurations are shown in Fig. 1. In these configurations, Fe^{3+} ions are ordered in (010) plane of the perovskite structure. The trend observed here is similar to the one noticed by (*Umemoto et al.*, 2008) for Fe^{2+} substitution in bridgmanite, where Fe^{2+} ions preferentially order in the (110)-plane. This observation suggests that Fe^{3+} substitution in bridgmanite prefers to cluster at lower mantle pressure conditions. For better understanding, this ordering effect should be investigated by sampling all possible configurations in very large super-cells and performing solid solution calculations. However, for practical reason we must limit ourselves to smaller super-cells here.

First, we investigate the effect of disordered substitution of Fe^{3+} in bridgmanite. For this purpose, the free-energy for HS/LS states of $[Fe^{3+}]_{Si}$ has been calculated using Eq. 4 by disregarding the vibrational contribution. The LS fraction, $n(P, T)$, shown in Fig. 3, was calculated using Eq. 9. $n(P, T)$ in the disordered system depends on the number of configurations (N_c)
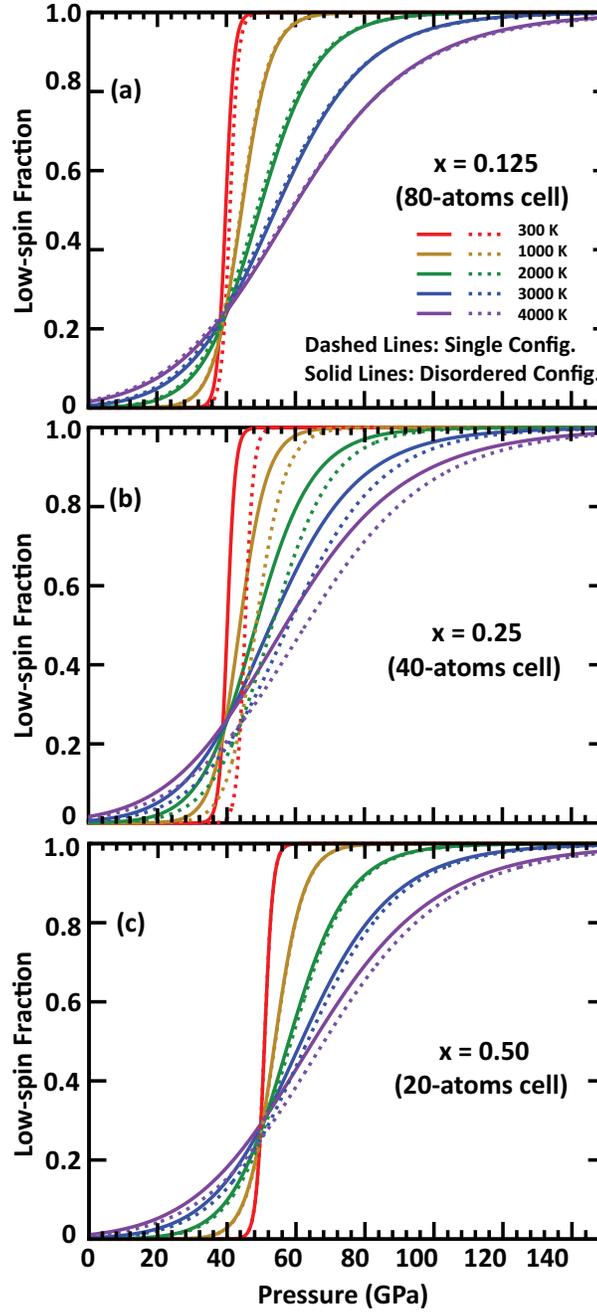
Figure 3: (Color online) Pressure and temperature dependence of low-spin fraction (n) of $[Fe^{3+}]_{Si}$ in $(Mg,Fe^{3+})(Si,Fe^{3+})O_3$ bridgmanite in a) 80 , (b) 40, and (c) 20 atom super-cells, respectively. Solid lines represent disordered configurations while dashed lines are for the lowest enthalpy configuration.
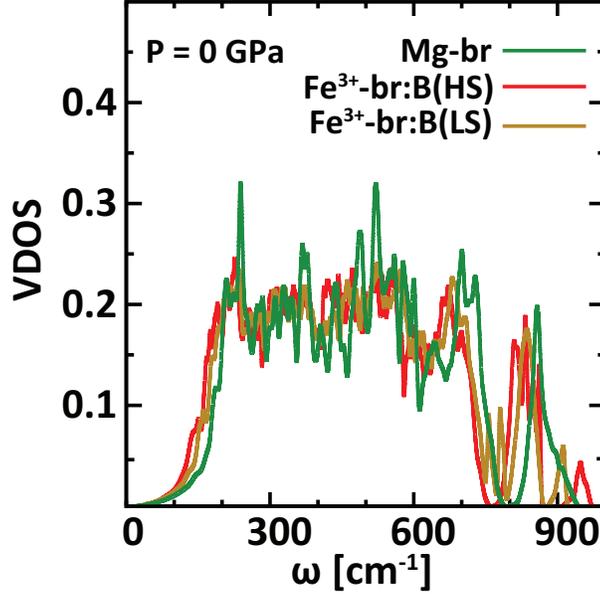
Figure 4: (Color online) Vibrational density of states (VDOS) at 0 GPa for MgSiO$_3$ bridgmanite (Mg-br) using DFPT method (*Baroni et al.*, 2001), and for HS and LS state states of [Fe^{3+}]$_{Si}$ (i.e, ferric iron in B-site of the perovskite structure) in Fe^{3+}-bearing bridgmanite (Fe^{3+}-br) using DFPT + U$_{sc}$ method (*Floris et al.*, 2011).

and their enthalpies. For x = 0.125, $n(P, T)$ in the disordered system (solid lines) at 300 K shifts towards the smaller pressure region compared to that of the lowest enthalpy configuration (dashed lines). This is caused by the contribution of the second lowest enthalpy configuration with smaller static crossover pressure (P$_T$) (Fig. 2a). At higher temperatures, the contribution from other configurations with higher enthalpy and higher P$_T$ shifts the disordered system's $n(P, T)$ towards higher pressures. The number of symmetrically inequivalent configurations decreases drastically with decreasing super-cell size. For x = 0.25 (40-atom super-cell), the lowest enthalpy configuration has the second highest P$_T$ (Fig. 2b). $n(P, T)$ for the disordered system is shifted to lower pressures due to contributions of configurations with smaller P$_T$ and enthalpy difference below ~25meV. In the case of x = 0.50 (20-atom super-cell), all configurations other than the lowest enthalpy one have much higher enthalpy and do not contribute significantly to change $n(P, T)$ of disordered system at lower temperatures. However, at higher temperatures ($\geq$ 2000 K) other configurations contribute to shift $n(P, T)$ towards smaller pressures (Fig. 2c). In overall, the crossover pressure increases significantly with increasing Fe^{3+} concentration, which is consistent with previous observations (*Lin et al.*, 2012; *Mao et al.*, 2015).

3.2. Effect of vibrations

Having investigated the effect of disorder, we now focus on vibrational effects. Owing to extremely high computational cost of vibrational density of states (VDOS) calculation) using LDA + U_{sc} functional, we have investigated vibrational effects only for the x = 0.125 system. VDOS calculation for HS/LS states of $[Fe^{3+}]_{Si}$ was performed in a 40-atoms super-cell. Example of these VDOS at 0 GPa are shown in Fig. 4. The VDOS spectrum for Fe^{3+}-br shifts towards lower frequencies with respect to that of $MgSiO_3$-bridgmanite (Mg-br) due to increased molecular weight of Fe^{3+}-br. The high frequency region of VDOS for the LS state of $[Fe^{3+}]_{Si}$ further shifts towards low frequency due to HS to LS crossover.

The vibrational contribution to the free-energy was calculated within the quasiharmonic approximation (QHA) (*Carrier et al.*, 2007; *Wallace*, 1972). The pressure and temperature dependence of calculated low-spin fraction, $n(P,T)$, is shown in Fig. 5. The orbital degeneracy for the LS state, m_{LS}, is more likely to be 1 due to octahedron asymmetry. However, in order to assess the effect of orbital degeneracy variation, calculated $n(P,T)$ for m_{LS} = 1 (dashed lines) are also compared with that for m_{LS} = 3 (solid lines). Inclusion of the vibrational contribution to free-energy increases the crossover pressure significantly. $n(P,T)$ for m_{LS} = 1 and 3 are also shown in Fig. 5(b) and in Fig. 5(c), respectively. In overall, $n(P,T)$ for m_{LS} = 1 and 3 are similar except for the difference in Clapeyron slopes (i.e., dP_T/dT for n = 0.5). Since the high temperature crossover broadening is not affected by the choice of m_{LS} values, we will continue this analysis using m_{LS} = 1. The spin crossover of $[Fe^{3+}]_{Si}$ shown here is much broader than that reported by *Tsuchiya and Wang* (2013). Our estimated crossover pressure width at 300 K is about ~8 GPa, which agrees fairly well with the experimental measurements (*Catalli et al.*, 2010; *Lin et al.*, 2012; *Mao et al.*, 2015), while the one reported by *Tsuchiya and Wang* (2013) is <2 GPa. These differences become more prominent at higher temperatures and may be related to the use of different values of Hubbard U and different techniques for VDOS calculations. The values of U used here were calculated self-consistently (*Cococcioni and de Gironcoli*, 2005) (i.e., starting form a trial LDA + U ground state, self-consistent U_{sc}'s are obtained iteratively), while those reported by *Tsuchiya and Wang* (2013) were calculated from LDA ground states. *Tsuchiya and Wang* (2013) used a finite displacement method (*Alfè*, 2009) to obtain their VDOS and disregarded the calculation of dielectric constant tensor that leads to LO-TO splitting for polar materials. In this work, we have used DFPT + U_{sc} method developed by *Floris et al.* (2011) for VDOS computation. Although computationally expensive, this method is a more precise approach for lattice dynamical calculations. This method has been applied successfully to address the lateral displacement of iron (a very delicate and highly debated phenomenon) and its associated change of Mössbauer quadrupole splitting (QS) in Fe^{2+}-bearing bridgmanite (*Shukla et al.*, 2015a). Therefore, we believe that calculation of VDOS and vibrational free-energy contribution using DFPT + U_{sc} method is quite robust.
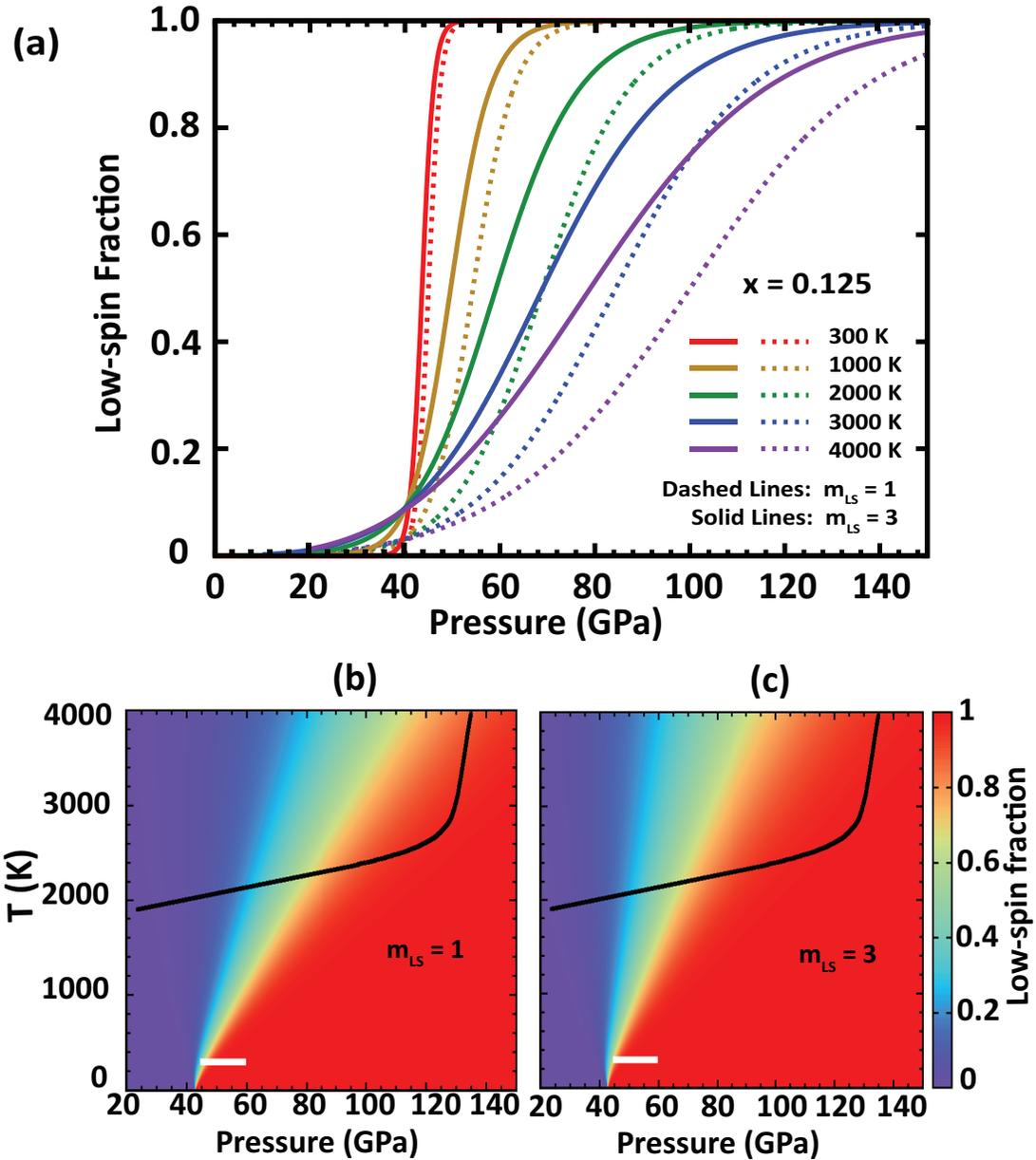
Figure 5: (Color online) (a) Low-spin fraction (n) of $[Fe^{3+}]_{Si}$ in $(Mg_{0.875}Fe_{0.125})(Si_{0.875}Fe_{0.125})O_3$ bridgmanite when vibrational effects are incorporated using quasiharmonic approximation (*Carrier et al.*, 2007). Dashed and solid lines represent the calculations for $m_{LS} = 1$ and 3, respectively. Pressure temperature phase diagram for HS to LS crossover of $[Fe^{3+}]_{Si}$ (b) with $m_{LS} = 1$, and (c) $m_{LS} = 3$. Solid black lines in (b and c) represents the lower mantle model geotherm by (*Boehler*, 2000), while white bar represents the experimental pressure range at room temperature in which HS to LS crossover of $[Fe^{3+}]_{Si}$ is completed (*Catalli et al.*, 2010).
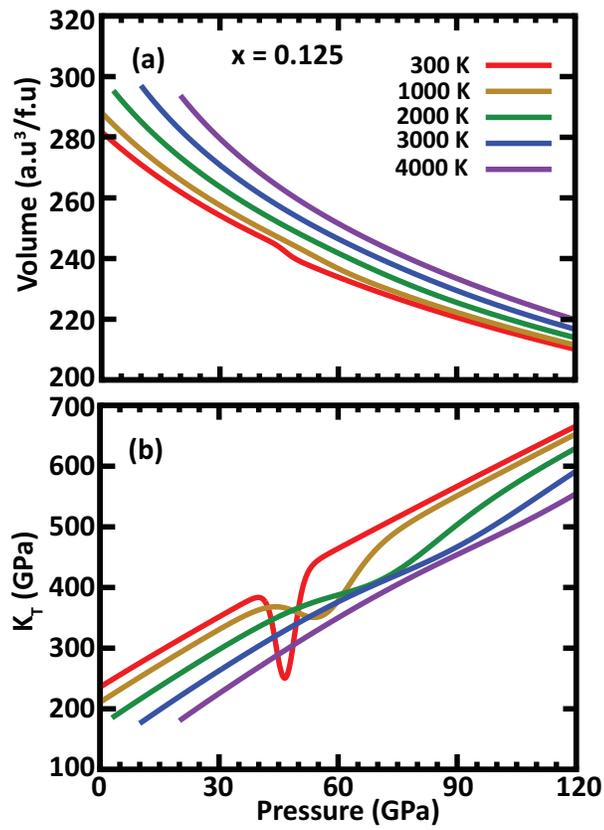
Figure 6: (Color online) Pressure and temperature dependence of (a) volume (per formula unit), and (b) isothermal bulk moduli for $(Mg_{0.875}Fe_{0.125})(Si_{0.875}Fe_{0.125})O_3$ bridgmanite.

4. Effect of spin crossover on volume and bulk modulus

4.1. Theoretical predictions

Spin crossover of $[Fe^{3+}]_{Si}$ in Fe^{3+}-br is quite sharp in the lower temperature region and broadens significantly at higher temperature (Fig. 5). To understand the consequences of this spin crossover on elastic properties, we used the solid solution formalism adopted by *Wentzcovitch et al.* (2009) to calculate volume and bulk modulus of the mixed spin state (MS):

$$V_{MS}(T, P) = (1 - n)V_{HS}(T, P) + nV_{LS}(T, P), \tag{10}$$

where n is the LS fraction. Using $K_T(T, P) = -V_{MS}(dP/dV_{MS})$, isothermal bulk modulus of MS state is given by

$$\frac{V_{MS}}{K_T} = n\frac{V_{LS}}{K_T^{LS}} + (1 - n)\frac{V_{HS}}{K_T^{HS}}$$
$$-(V_{LS} - V_{HS})\frac{\partial n}{\partial P}\bigg|_T, \tag{11}$$

where $K_T^{HS/LS}$ are the isothermal bulk moduli of HS/LS states.

The HS to LS crossover of $[Fe^{3+}]_{Si}$ goes through volume reduction, which produces anomalous softening in the bulk modulus (K) in the crossover region. The strength of the anomaly depends on temperature, volume difference ($\Delta V^{HS \to LS} = V_{LS} - V_{HS}$), and Gibb's free-energy difference ($\Delta G^{HS \to LS} = G_{LS} - G_{HS}$). For $x = 0.01$, $\Delta V^{HS \to LS}$ is approximately ~-0.15%, which agrees well with results of previous first-principles calculations (*Hsu et al.*, 2011; *Tsuchiya and Wang*, 2013) and is fairly comparable to the experimental value of ~-0.2% (*Mao et al.*, 2015). This volume reduction produces a significant bulk modulus softening (~12%) at 300 K, which is smeared out with increasing temperature due to broadening of the spin crossover region (Fig. 6b). In spite of the clear volume reduction throughout the spin crossover, *Tsuchiya and Wang* (2013) disregarded the anomalous softening of bulk modulus probably due to very sharp crossover observed in their calculations. However, owing to the considerably broad HS to LS crossover and noticeable volume reduction, as evidenced by experimental measurements (*Mao et al.*, 2015), this spin crossover should also be accompanied by a bulk modulus softening anomaly.

4.2. Comparison with experiments

Having calculated the compression curves for Fe^{3+}-br, we compare our results with the available experimental measurements. Our calculated compression curves for pure $MgSiO_3$, $(Mg_{1-x}Fe_x^{2+})SiO_3$, and $(Mg_{1-x}Fe_x^{3+})(Si_{1-x}Fe_x^{3+})O_3$, shown in Fig. 7a, 7b, and 7c, respectively, agree well with measurements (*Fiquet et al.*, 2000; *Vanpeteghem et al.*, 2006; *Lundin et al.*, 2008; *Catalli et al.*, 2010; *Boffa Ballaran et al.*, 2012; *Chantel et al.*, 2012). Compression curves for $0 < x < 0.125$ are linearly interpolated using $x = 0$ and 0.125 results. Using enstatite powder, $(Mg_{0.9}Fe_{0.1})SiO_3$, bridgmanite (Br10) was synthesized by *Lin et al.* (2012) and it was suggested that sample may have $Fe^{3+}/\sum Fe \approx 20\%$ in the octahedral sites (Si-sites) and $Fe^{2+}/\sum Fe \approx 80\%$ in the Mg-sites. Compression curve for this sample at 300 K was recently obtained by *Mao et al.* (2015).

In order to gradually transform Fe^{2+} to Fe^{3+} in the sample under pressure, the system should at least be able to 1) incorporate MgO and O_2, 2) produce metallic iron, 3) create vacancies, or 4) a combination of these (*Xu et al.*, 2015). *Lin et al.* (2012) synthesis seems to be in a closed system, where Fe^{3+} production from Fe^{2+} is more likely to be accompanied by Mg and O vacancies. Therefore to compare with measurements by *Mao et al.* (2015), we modeled their Br10 sample as

$$
\begin{aligned}
Br10 = (Mg_{0.9}Fe_{0.1})SiO_3 \quad = \quad & a(Mg_{1-x}Fe_x^{2+})SiO_{(3)} \\
+ \quad & b(Mg_{1-y-\alpha}Fe_y^{3+})(Si_{1-y}Fe_y^{3+})O_{3(1-\beta)},
\end{aligned}
\tag{12}
$$

where stoichiometric coefficients are constrained by $ax + 2by = 0.1$, $\alpha = 2y$, and $\beta = y$. (see Appendix A).

These products containing Mg and O vacancies ($[V]_{Mg}$ and $[V]_O$) should be created in the absence of other phases in a closed system. It is important, therefore, to investigate the effect of vacancies on compression curves. Fig. 8(a) compares the static compression curves for pure $MgSiO_3$, $(Mg_{1-x}Fe_x^{2+})SiO_3$, and $(Mg_{1-3x/2}Fe_x^{3+})SiO_3$. Fe^{3+} in $(Mg_{1-3x/2}Fe_x^{3+})SiO_3$ is accommodated exclusively in Mg-site via Mg vacancies ($3Mg^{2+} \rightarrow 2[Fe^{3+}]_{Mg} + [V]_{Mg}$). The presence of $[Fe^{2+}]_{Mg}$ and $[Fe^{3+}]_{Mg}$ in the perovskite A-site alone do not affect the compression curve significantly. The dominant changes in the compression curve are due to $[Fe^{3+}]_{Si}$. Therefore, the compression curve for our model Br10 (Eq. 12), where Fe^{3+} is accommodated via coupled substitution $[Fe^{3+}]_{Mg}$-$[Fe^{3+}]_{Si}$ with Mg and O vacancies, would be a reasonably close to the one obtained by *Mao et al.* (2015). We calculated the compression curves for our model Br10 with $10\% \leq [Fe^{3+}]_{Si}/\sum Fe \leq 20\%$. Stoichiometric coefficients in Eq. 12 for 10% $[Fe^{3+}]_{Si}/\sum Fe$ (lower-bound) are: a = b = 0.505, x = 0.15842, y = 0.019802, and for 20% $[Fe^{3+}]_{Si}/\sum Fe$ (upper-bound) are: a = b = 0.51, x = 0.11765, y = 0.039216. Details of these stoichiometry calculations are shown in Appendix A. It is worth mentioning here that the total iron concentration in our B10 model is fixed and any variation in $[Fe^{3+}]_{Si}$ will be constrained by simultaneous changes in $[Fe^{3+}]_{Mg}$ and $[Fe^{2+}]_{Mg}$. As shown in Fig. 8(b), the compression curve of $Mg_{1-x}SiO_{3(1-x/3)}$ with $x = 0.03125$ (i.e., $MgSiO_3$ with small amount of Mg and O vacancies) is very similar to that of pure $MgSiO_3$. Therefore, we use

$$
\begin{aligned}
Br10 = (Mg_{0.9}Fe_{0.1})SiO_3 \quad \approx \quad & a(Mg_{1-x}Fe_x^{2+})SiO_3 \\
+ \quad & b(Mg_{1-y}Fe_y^{3+})(Si_{1-y}Fe_y^{3+})O_3,
\end{aligned}
\tag{13}
$$

as approximate description of Eq. (12). Calculated 300 K compression curve for model Br10 is depicted by red curve in Fig. 9. *Mao et al.* (2015) data for compression curve (black symbols) tends to agree better with the calculated values for $(Mg_{0.9}Fe_{0.1}^{2+})SiO_3$ in the lower-pressure range, while in the higher-pressure range agreement with our model Br10 (red curve) is better. This observation suggests that Fe^{2+} present in the sample at ambient condition may tend to transform into Fe^{3+} with increasing pressure.

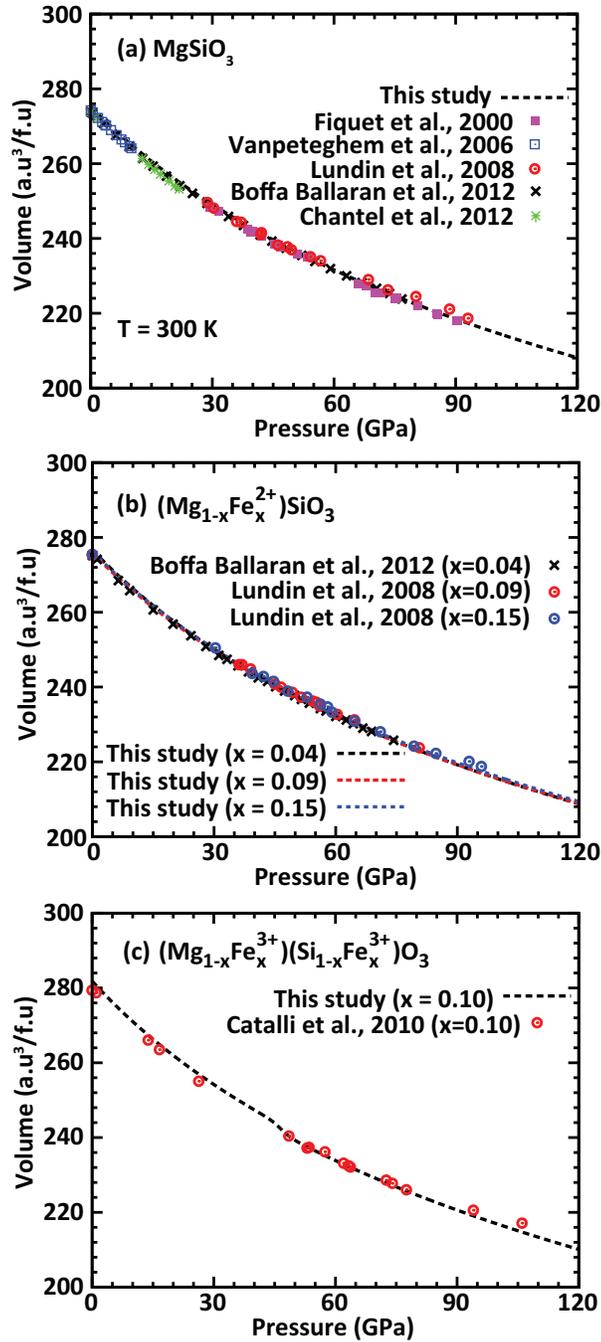Figure 7: (Color online) 300 K compression curves for (a) $MgSiO_3$, (b) $(Mg_{1-x}Fe_x^{2+})SiO_3$, and (c) $(Mg_{1-x}Fe_x^{3+})(Si_{1-x}Fe_x^{3+})O_3$. Our first-principles calculations (lines) are compared with experimental measurements (symbols).

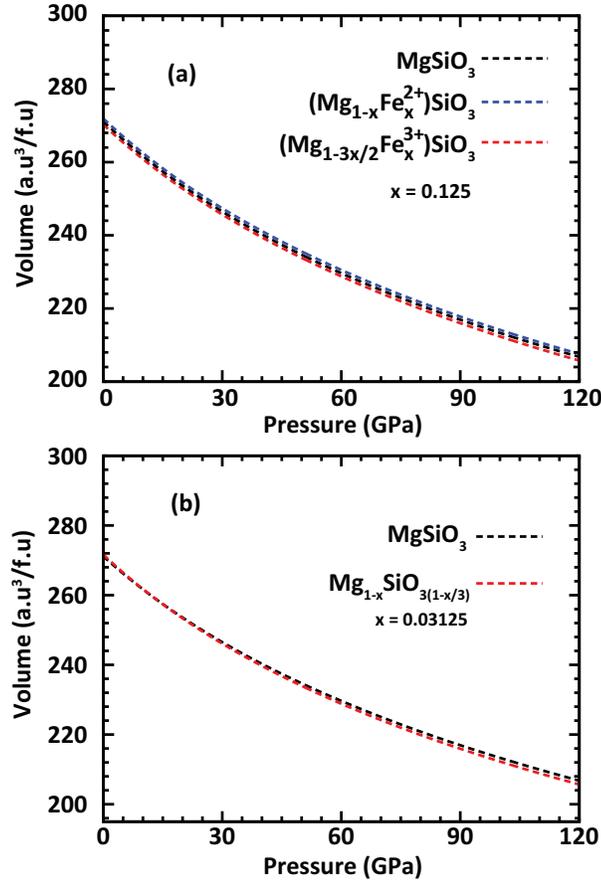Figure 8: (Color online) Static compression curves comparison of (a) $MgSiO_3$ and $(Mg_{1-3x/2}Fe_x^{3+})SiO_3$ ($x = 0.125$) and (b) $MgSiO_3$ and $Mg_{1-x}SiO_{3(1-x/3)}$ ($x = 0.03125$).

Two clarifications are in order: first, the larger volume of Br10 beyond approximately 45 GPa, compared to that of $(Mg_{0.9}Fe_{0.1}^{2+})SiO_3$ or $(Mg_{0.95}Fe_{0.05}^{3+})Si_{0.95}Fe_{0.05}^{3+}O_3$ is achieved by the introduction of vacancies while maintaining the number of moles of each element invariant; second, such conclusion is achieved exclusively on the basis of the compression curve. No energetics has been investigated yet, the main reason being the nature of these vacancies is unclear. There are multiple possibilities, including Mg-O vacancy ordering associated with Fe^{3+}. This is not uncommon in transition metal oxides (*Schulz and Wentzcovitch*, 1993; *Leung et al.*, 1996) where the metal has multiple valences, iron in this case. Theoretical investigation of this problem is highly desirable but a non-trivial task that goes beyond the scope of this work.
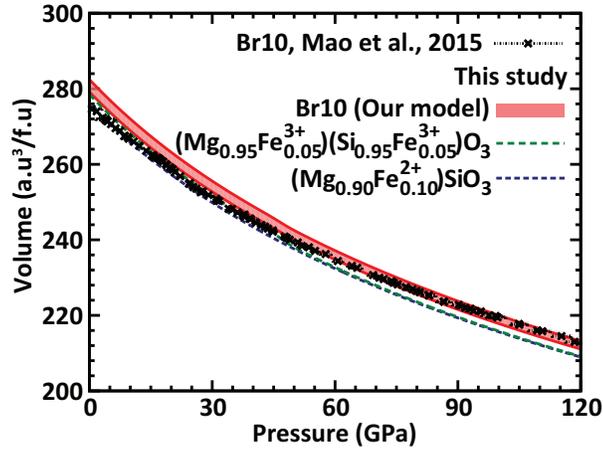
Figure 9: (Color online) Compression curve for bridgmanite with 10 mol.% Fe (Br10). Our first-principles calculations (lines and red filed-curve) are compared with experimental measurements (black symbols). Br10 sample was synthesized by *Lin et al.* (2012) and compression curve was measured by *Mao et al.* (2015). Here, Br10 sample has been been modeled by balancing the stoichiometry with appropriate molar fractions of $(Mg_{1-x}Fe_x^{2+})SiO_3$ and $(Mg_{1-x}Fe_x^{3+})(Si_{1-x}Fe_x^{3+})O_3$ bridgmanite (red filed-curve). Lower- and upper-bounds of the compression curve are for 10% and 20% $[Fe^{3+}]_{Si}/\sum Fe$ in the sample, respectively.

5. Geophysical Significance

The bulk modulus of $(Mg_{1-x}Fe_x^{3+})(Si_{1-x}Fe_x^{3+})O_3$ along a lower mantle model geotherm (*Boehler*, 2000) (black lines in Fig. 5b and 5c) for several Fe^{3+} concentrations are shown in Fig. 10. For x = 0.125, the bulk modulus softening for Fe^{3+}-br (~7%) is smaller than that for (Mg,Fe)O (~11%) (*Wu et al.*, 2013). This anomaly reduces rapidly with decreasing *x* and almost disappears for *x* = 0.02 concentration. Based on a thermodynamics model, *Xu et al.* (2015) estimated the amount of $Fe^{3+}/\sum Fe$ to be very small (~0.01-0.07) in Al-free bridgmanite under lower mantle conditions. Considering this fact, the spin crossover of $[Fe^{3+}]_{Si}$ in bridgmanite may not have the same noticeable impact on lower mantle properties as in (Mg,Fe)O ferropericlase (*Wu and Wentzcovitch*, 2014). Nevertheless, the volume reduction and its associated elastic anomalies due to HS and LS crossover of $[Fe^{3+}]_{Si}$ should be taken into account in calculations of thermodynamic equilibrium in the lower mantle.

6. Conclusions

We have presented a first-principles LDA + U_{sc} investigation of the spin crossover in $(Mg,Fe^{3+})(Si,Fe^{3+})O_3$ bridgmanite. In order to investigate the system close to experimental conditions, a disordered substitution of Fe^{3+} was modeled using complete sampling of configurations in super-cells containing up to 80 atoms. Thermal effects were properly captured by calculating the vibrational contribution to the free-energy within the quasi harmonic approximation. Disorder of Fe^{3+} does not seem to affect the HS to LS crossover of $[Fe^{3+}]_{Si}$ significantly. The crossover pressure increases with increasing Fe^{3+} concentration, which
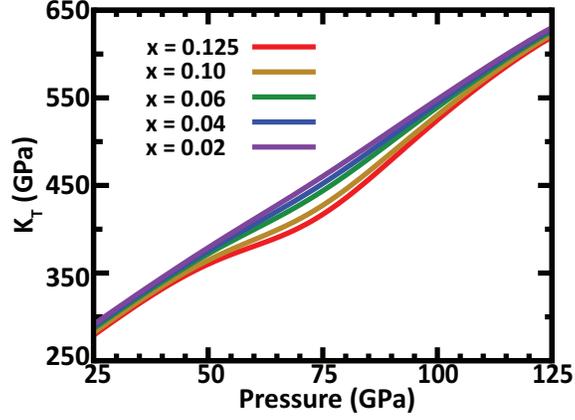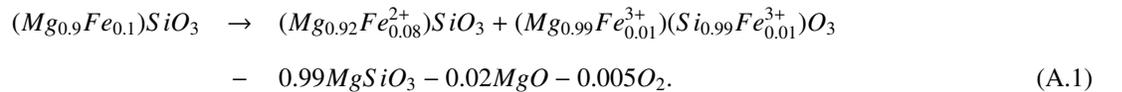
Figure 10: (Color online) Bulk moduli (K_T) for $(Mg_{1-x}Fe_x^{3+})(Si_{1-x}Fe_x^{3+})O_3$ bridgmanite along the Earth's lower mantle geotherm (*Boehler*, 2000) for varying Fe^{3+} concentration.

is consistent with experimental observations (*Lin et al.*, 2012; *Mao et al.*, 2015). Comparison of our calculated compression curves with that of *Mao et al.* (2015) suggests that in a closed system, Fe^{2+} present in the sample may tend to transform into Fe^{3+} by introduction of Mg and O vacancies with increasing pressure, whose arrangements is still unclear. The spin crossover is also accompanied by a significant volume reduction and by an anomalous decrease in the bulk modulus across the crossover region, in contrast with previous calculations. Further investigations of the effect of the spin crossover on elastic properties at lower mantle conditions are needed to better understand the thermal structure and the composition of the Earth's lower mantle. The present study establishes a foundation for such study.

Appendix A. Solid solution model for Br10 sample

Here, we describe the Br10 model which has been used to analyze the compression curve obtained by *Mao et al.*, 2015 for the bridgmanite sample (Br10) containing $Fe^{3+}/\sum Fe \approx 20\%$ in the octahedral sites (Si-sites) and $Fe^{2+}/\sum Fe \approx 80\%$ in the Mg-sites. We model Br10 by balancing the stoichiometry with appropriate molar fractions of $(Mg_{1-x}Fe_x^{2+})SiO_3$ and $(Mg_{1-x}Fe_x^{3+})(Si_{1-x}Fe_x^{3+})O_3$ bridgmanite. We vary $Fe_{Si}^{3+}/\sum Fe$ from 10% to 20% to assess the effect of Fe^{3+} variation on the compression curve. The volume of Br10 is modeled using an ideal solid solution between Fe^{2+}- and Fe^{3+}-bearing bridgmanite.

The stoichiometry for the sample containing 10% $Fe_{Si}^{3+}/\sum Fe$ (lower bound) is obtained as follows:

$$
\begin{aligned}
(Mg_{0.9}Fe_{0.1})SiO_3 \quad \rightarrow \quad & (Mg_{0.92}Fe_{0.08}^{2+})SiO_3 + (Mg_{0.99}Fe_{0.01}^{3+})(Si_{0.99}Fe_{0.01}^{3+})O_3 \\
- \quad & 0.99MgSiO_3 - 0.02MgO - 0.005O_2.
\end{aligned}
\tag{A.1}
$$

17

Transferring equal amount of $MgSiO_3$ to both Fe^{2+}- and Fe^{3+}-bearing $MgSiO_3$, we obtain

$$
\begin{aligned}
(Mg_{0.9}Fe_{0.1})SiO_3 \quad \rightarrow \quad & \left[(Mg_{0.92}Fe^{2+}_{0.08})SiO_3 - 0.495MgSiO_3 \right] \\
+ \quad & \left[(Mg_{0.99}Fe^{3+}_{0.01})(Si_{0.99}Fe^{3+}_{0.01})O_3 - 0.495MgSiO_3 \right] \\
- \quad & 0.02MgO - 0.005O_2,
\end{aligned}
\tag{A.2}
$$

or

$$
\begin{aligned}
(Mg_{0.9}Fe_{0.1})SiO_3 \quad \rightarrow \quad & 0.505(Mg_{0.84158}Fe^{2+}_{0.15842})SiO_3 \\
+ \quad & 0.505(Mg_{0.9802}Fe^{3+}_{0.019802})(Si_{0.9802}Fe^{3+}_{0.019802})O_3 \\
- \quad & 0.02MgO - 0.005O_2.
\end{aligned}
\tag{A.3}
$$

We chose to incorporate MgO and O_2 as Mg and O vacancies in Fe^{3+}-bearing $MgSiO_3$:

$$
\begin{aligned}
(Mg_{0.9}Fe_{0.1})SiO_3 \quad \rightarrow \quad & 0.505(Mg_{0.84158}Fe^{2+}_{0.15842})SiO_3 \\
+ \quad & 0.505 \left[(Mg_{0.9802}Fe^{3+}_{0.019802})(Si_{0.9802}Fe^{3+}_{0.019802})O_3 \right. \\
- \quad & \left. 0.039604Mg - 0.059406O \right].
\end{aligned}
\tag{A.4}
$$

The above equation can be rearranged as

$$
\begin{aligned}
(Mg_{0.9}Fe_{0.1})SiO_3 \quad \rightarrow \quad & a(Mg_{1-x}Fe^{2+}_x)SiO_3 \\
+ \quad & b(Mg_{1-y-\alpha}Fe^{3+}_y)(Si_{1-y}Fe^{3+}_y)O_{3(1-\beta)},
\end{aligned}
\tag{A.5}
$$

where Mg and O vacancies are constrained by Fe^{3+} concentration as $\alpha = 2y$ and $\beta = y$. Owing to the fact that the total iron concentration in the sample is fixed, these stoichiometric coefficients are also constrained by $ax + 2by = 0.1$. For the sample containing 10% $[Fe^{3+}]_{Si}/\sum Fe$ (lower bound): $a = b = 0.505$, $x = 0.15842$, and $y = 0.019802$. Similarly for 20% $[Fe^{3+}]_{Si}/\sum Fe$ (upper bound): $a = b = 0.51$, $x = 0.11765$, $y = 0.039216$.

It is worth mentioning that the choice of the stoichiometric coefficients a and b in Eq. A.5 is not unique. However, since the volume variation with respect to iron substitution in bridgmanite has been assumed to be linear and we are assuming an ideal solid solution of Fe^{2+}- and Fe^{3+}-bearing bridgmanite, other choices of a and b would provide the same estimate for the compression curve of our B10 model.

Acknowledgments

References

References

Alfè, D. (2009), PHON: A program to calculate phonons using the small displacement method, *Comp. Phys. Commun.*, *180*, 26222633, doi:10.1016/j.cpc.2009.03.010.

Antonangeli, D., J. Siebert, C. M. Aracne, D. L. Farber, A. Bosak, M. Hoesch, M. Krisch, F. J. Ryerson, G. Fiquet, and J. Badro (2011), Spin Crossover in Ferropericlase at High Pressure: A Seismologically Transparent Transition?, *Science*, *331*, 64-67.

Badro J., G. Fiquet, F. Guyot, J. P. Rueff, V. V. Struzhkin, G. Vank, and G. Monaco (2003), Iron Partitioning in Earth's Mantle: Toward a Deep Lower Mantle Discontinuity, *Science*, *300*, 789-791.

Badro J., J. P. R ueff, G. Vanko, G. Monaco, G. Fiquet, and F. Guyot (2004), Electronic Transitions in Perovskite: Possible Nonconvecting Layers in the Lower Mantle, *Science*, *305*, 383.

Baroni, S., A. Dal Corso, S. de Gironcoli, and P. Gianozzi (2001), Phonons and related crystal properties from density-functional perturbation theory, *Rev. Mod. Phys.*, *73(2)*, 515LP–565LP.

Bengtson, A., J. Li, and D. Morgan (2009), Mössbauer modeling to interpret the spin sate of iron in (Mg,Fe)SiO$_3$, *Geophys. Res. Lett.*, *36*, L15301, doi:10.1029/2009GL038340.

Boehler, R. (2000), High-pressure experiments and the phase diagram of lower mantle and core materials, *Rev. Geophys.*, *38(2)*, 221–245.

Boffa Ballaran, T., A. Kurnosov, K. Glazyrin, D. J. Frost, M. Merlini, M. Hanfland, and R. Caracas (2012), Effect of chemistry on the compressibility of silicate perovskite in the lower mantle, *Earth Planet. Sci. Lett.*, *333-334*, 181–190, doi:10.1016/j.epsl.2012.03.029.

Caracas, R., H. Ishii , M. Hiraoka, Y. Ohishi, and N. Hirao (2014), Identifying the spin transition in Fe^{2+}-rich MgSiO$_3$ perovskite from X-ray diffraction and vibrational spectroscopy , *American Mineralogist*, *99(7)*, 1270–1276, doi:10.2138/am.2014.4783.

Carrier, P., R. M. Wentzcovitch, and J. Tsuchiya (2007), First principles prediction of crystal structures at high temperatures using the quasiharmonic approximation, *Phys. Rev. B*, *76*, 064116, doi:10.1103/PhysRevB.76.064116.

Catalli, K., S.-H. Shim, V. B. Prakapenka, J. Zhao, W. Sturhahn, P Chow, Y. Xiao, H. Liu, H. Cynn, and W.J. Evans (2010a), Spin state of ferric iron in MgSiO$_3$ perovskite and its effect on elastic properties, *Earth Planet. Sci. Lett. *, *289*, 68–75.

Ceperley, D. M., and B. J. Alder (1980), Ground state of the electron gas by a stochastic method, *Phys. Rev. Lett.*, *45*, 566–569.

Chantel, J., D. J. Frost,C. A. McCammon, Z. Jing, and Y. Wang (2012), Acoustic velocities of pure and iron-bearing magnesium silicate perovskite measured to 25 GPa and 1200 K, *Geophys. Res. Lett.*, *39*, L19307, doi:10.1029/2012GL053075, 2012.

Cococcioni, M., and S. de Gironcoli (2005), Linear response approach to the calculation of the effective interaction parameters in the LDA + U method, *Phys. Rev. B*, *71*, 035105.

Crowhurst, J. C., J. M. Brown, A. F. Goncharov, and S. D. Jacobsen (2008), Elasticity of (Mg,Fe)O through the spin transition of iron in the lower mantle, *Science*, *319*, 451–453, doi:10.1126/science.1149606.

da Silva, P., C. R. S. da Silva and R. M. Wentzcovitch (2008), Metadata management for distributed first principles calculations in VLab - A collaborative cyberinfrastructure for materials computation, *Comp. Phys. Comm.*, *178*, 186, doi:10.1016/j.cpc.2007.09.001.

Dorfman, S. M., Y. Meng, V. B. Prakapenka, and T. S. Duffy (2013), Effects of Fe-enrichment on the equation of state and stability of (Mg,Fe)SiO$_3$ perovskite, *Earth Planet. Sci. Lett.*, *361*, 249–257.

Dubrovinsky, L., T. Boffa-Ballaran , K. Glazyrin , A. Kurnosov , D. Frost , M. Merlini , M. Hanfland , V.B. Prakapenka , P. Schouwink , T. Pippinger, and N. Dubrovinskaia (2010), Single-crystal X-ray diffraction at megabar pressures and temperatures of thousands of degrees, *High Pressure Research*, *30(4)*, 620–633.

Fei, Y., L. Zhang, A. Corgne, H. Watson, A. Ricolleau, Y. Meng, and V. Prakapenka (2007), Spin transition and equations of state of (Mg,Fe)O solid solutions, *Geophys. Res. Lett*, *34*, L17307.

Fiquet, G., A. Dewaele, D. Andrault, M. Kunz, and T. L. Bihan (2000), Thermoelastic properties and crystal structure of MgSiO$_3$ perovskite at lower mantle pressure and temperature conditions, *Geophys. Res. Lett.*, *27(1)*, 21–24.

Floris, A., S. de Gironcoli, E. K. U. Gross, and M. Cococcioni (2011), Vibrational properties of MnO and NiO from DFT +U-based density functional perturbation theory, *Phys. Rev. B*, *84*, 161102(R).

Frost, D. J., C. Liebske, F. Langenhorst, C. A. McCammon, R. G. TrØnnes, and D. C. Rubie (2004), Experimental evidence for the existence of iron-rich metal in the Earth's lower mantle, *Nature*, *428*, 409–412.

Fujino, K., D. Nishio-Hamane, Y. Seto, N. Sata, T. Nagai, T. Shinme, T. Irifune, H. Ishii, N. Hiraoka, Y. Q. Cai, K. D. Tsue (2012), Spin transition of ferric iron in Al-bearing Mgperovskite up to 200 GPa and its implication for the lower mantle, *Earth Planet. Sci. Lett.*, *317-318*, 407–412.

Goncharov, A. F., V. V. Struzhkin, and S. D. Jacobsen (2006), Reduced Radiative Conductivity of Low-Spin (Mg,Fe)O in the Lower Mantle, *Science*, *312*, 1205–1208, doi:10.1126/science.1125622.

Hsu, H., K. Umemoto, M. Cococcioni, and R. M. Wentzcovitch (2009), First principles study of low-spin LaCoO3 with structurally consistent Hubbard U, *Phys. Rev. B*, *79*, 125124, doi:10.1103/PhysRevB.79.125124.

Hsu, H., K. Umemoto, R. M. Wentzcovitch, and P. Blaha (2010), Spin states and hyperfine interactions of iron in (Mg,Fe)SiO$_3$ perovskite under pressure, *Earth Planet. Sci. Lett.*, *294*, 19–26, doi:10.1016/j.epsl.2010.02.031.

Hsu, H., P. Blaha, M. Cococcioni, and R. M. Wentzcovitch (2011), Spin-state crossover and hyperfine interactions of ferric iron in MgSiO$_3$ perovskite, *Phys. Rev. Lett.*, *106*, 118501, doi:10.1103/PhysRevLett.106.118501.

Hsu, H., and R. M. Wentzcovitch (2014), First-principles study of intermediate-spin ferrous iron in the Earth's lower mantle, *Phys. Rev. B*, *90(19)*, 195205, doi:10.1103/PhysRevB.90.195205.

Hummer, D. R., and Y. Fei (2012), Synthesis and crystal chemistry of Fe^{3+}-bearing (Mg,Fe^{3+})(Si,Fe^{3+})O$_3$ perovskite, *American Mineralogist*, *97*, 1915–2012.

Jackson, J.M., W. Sturhahn, G. Shen, J. Zhao, M. Y. Hu, D. Errandonea, J. D. Bass, and Y. Fei (2005a), A synchrotron Mössbauer spectroscopy study of (Mg,Fe)SiO$_3$ perovskite up to 120 GPa, *Am. Mineral.*, *90*, 199–205.

Kulik, H., M. Cococcioni, D. A. Scherlis, and N. Marzari (2006), Density functional theory in transition metal chemistry: a self-consistent Hubbard U approach, *Phys. Rev. Lett.*, *97*, 103001.

Kupenko, I., C. McCammon, R. Sinmyo, C. Prescher, A. I. Chumakov, A. Kantor,R. Rüffer, and D. Dubrovinsky(2014), Electronic spin state of Fe,Al-containing MgSiO$_3$ perovskite at lower mantle conditions , *Lithos*, *189*, 167–172 doi:10.1016/j.lithos.2013.10.022.

Leung, C., M. Weinert, P. B. Allen, and R. M. Wentzcovitch (1996), First principles study of titanium oxides, *Phys. Rev. B*, *54*, 7857.

Li, J., V. V. Struzhkin, H. K. Mao, J. Shu, R. J. Hemley, Y. Fei, B. Mysen, P. Dera, V. Prakapenka, and G. Shen (2004), Electronic spin state of iron in lower mantle perovskite, *Proc. Natl. Acad. Sci.*, *101*, 14027–14030.

Li, J., W. Sturhahn, J. M. Jackson, V. V. Struzhkin, J. F. Lin, J. Zhao, H. K. Mao, and G. Shen (2006), Pressure effect on the electronic structure of iron in (Mg,Fe)(Si,Al)O$_3$ perovskite: A combined synchrotron Mössbauer and X-ray emission spectroscopy study up to 100 GPa, *Phys. Chem. Minerals*, *33*, 575–585.

Lin, J., H. Watson, G. Vanko, E. E. Alp, V. B. Prakapenka, P. Dera, V. V. Struzhkin, A. Kubo, J. Zhao, C. McCammon, and W. J. Evans (2008), Intermediate-spin ferrous iron in lowermost mantle post-perovskite and perovskite, *Natl. Geosci*, *1*, 688–691.

Lin, J. F., E. E. Alp, Z. Mao, T. Inoue, C. McCammon, Y. Xiao, P. Chow, and J. Zhao (2012), Electronic spin and valence states of iron in the lower-mantle silicate perovskite by synchrotron Mssbauer spectroscopy, *American Mineralogist*, *97*, 592–597.

Lin, J. F., S. Speziale, Z. Mao, and H. Marquardt (2013), Effects of the electronic spin transitions of iron in lower-mantle minerals: implications to deep-mantle geophysics and geochemistry, *Rev. Geophys.*, *51*, 244–275.

Lundin, S., L. Catalli, J. Santillan, S.-H. Shim, V. B. Prakapenka, M. Kunz, and Y. Meng (2008), Effect of Fe on the equation of state of mantle silicate perovskite over 1 Mbar, *Phys. Earth Planet. Inter.*, *168*, 97–102.

Mao, Z., J.-F. Lin, J. Liu, and V. B. Prakapenka (2011), Thermal equation of state of lower-mantle ferropericlase across the spin crossover, *Geophys. Res.Lett.*, *38*, L23308.

Mao, Z., J.-F. Lin, J. Yang, T. Inoue, and V. B. Prakapenka (2015), Effects of the Fe^{3+} spin transition on the equation of state of bridgmanite, *Geophys. Res.Lett.*, *42*, 4335–4342.

Marquardt M., S. Speziale, H. J. Reichmann, D. J. Frost, F. R. Schilling, and E. J. Garnero (2009), Elastic Shear Anisotropy of Ferropericlase in Earth's Lower Mantle, *Science*, *324*, 224–226, doi:10.1126/science.1169365.

McCammon, C., I. Kantor, O. Narygina, J. Rouquette, U. Ponkratz, I. Sergueev, M. Mezouar, V. Prakapenka, and L. Dubrovinsky (2008), Stable intermediate-spin ferrous iron in lower-mantle perovskite, *Nat. Geosci.*, *1*, 684–687.

McCammon, C., L. Dubrovinsky, O. Narygina, I. Kantor, X. Wu, K. Glazyrin, I. Sergueev, and A. I Chumakov (2008), Low-spin Fe^{2+} in silicate perovskite and a possible layer at the base of the lower mantle, *Phys. Earth Planet. Inter.*, *180*, 215–221.

McCammon, C., K. Glazyrin, A. Kantor, I. Kantor, I. Kupenko, O. Narygina, V. Potapkin, C. Prescher, R. Sinmyo, A. Chumakov, R. R*ü*ffer, I. Sergueev, G. Smirnov, and L. Dubrovinsky (2013), Iron spin state in silicate perovskite at conditions of the Earth's deep interior, *High Press. Res.*, *43(3)*, 663–672.

Potapkin, V, C. McCammon, K. Glazyrin, A. Kantor, I. Kupenko, C. Prescher, R. Sinmyo, G. V. Smirnov, A. I. Chumakov, R. R*ü*ffer, and L. Dubrovinsky (2013), Effect of iron oxidation state on the electrical conductivity of the Earth's lower mantle , *Nature Communication*, *4*,1427.

Shukla, G., Z. Wu, H. Hsu, A. Floris, M. Cococcioni, and R. M. Wentzcovitch (2015), Thermoelasticity of Fe^{2+}-bearing bridgmanite, *Geophys. Res. Lett.*, *42*, 1741-1749.

Shukla, G., M. Topsakal, and R. M. Wentzcovitch (2015), Spin crossovers in iron-bearing $MgSiO_3$ and $MgGeO_3$: Their influence on the post-perovskite transition, *Phys. Earth Planet. Inter.*, *249*, 11–17.

Sinmyo R., E. Bykova, C. McCammon, I Kupenko, VPotapkin , and L. Dubrovinsky (2014), Crystal chemistry of Fe^{2+} bearing (Mg,Fe)SiO3 perovskite: a singlecrystal Xray diffraction study, *Phys. Chem. Minerals*, *41*, 409-417.

Stackhouse, S., J. P. Brodholt, and G. D. Price (2007), Electronic spin transitions in iron-bearing $MgSiO_3$ perovskite, *Earth Planet. Sci. Lett.*, *253*, 282–290.

Schulz, W. W., and R. M. Wentzcovitch (1993), Electronic structure and bonding in Nb_3O_3, *Phys. Rev. B*, *48*, 16986.

Tsuchiya, T., R. M. Wentzcovitch, C. R. S. da Silva, S. de Gironcoli (2006), Spin transition in magnesiowstite in Earth's lower mantle, *Phys. Rev. Lett.*, *96(19)*, 198501.

Tsuchiya, T., and X. Wang (2013), Ab initio investigation on the high-temperature thermodynamic properties of Fe^{3+}-bearing $MgSiO_3$ perovskite, *J. Geophys. Res. Solid Earth*, *118*, 83–91.

Umemoto, K., R. M. Wentzcovitch, Y. Yu, and R. Requist (2008), Spin transition in $(Mg,Fe)SiO_3$ perovskite under pressure, *Earth Planet. Sci. Lett.*, *276*, 198–206, doi:10.1016/j.epsl.2008.09.025.

Umemoto, K., R. M. Wentzcovitch, S. de Gironcoli, and S. Baroni (2010), Orderdisorder phase boundary between ice VII and VIII obtained by first principles, *Chem. Phys. Lett.*, *499*, 236–240.

Vanderbilt, D., (1990), Soft self-consitent pseudopotentials in a genrelized eigenvalue formalism, *Phys. Rev. B*, *41*, 7892–7895.

Vanpeteghem, C.B., J. Zhao, R. J. Angel, N. L. Ross, and N. Bolfan-Casanova (2006), Crystal structure and equation of state of $MgSiO_3$ perovskite, *Geophys. Res. Lett.*, *33*, L03306.

Wallace, D. C., (1972), Thermodynamic of Crystals, John Wiley & Sons, Inc., USA.

Wentzcovitch, R. M., (1991), Invariant molecular dynamics approach to structural phase transitions, *Phys. Rev. B*, *44*, 2358-2361.

Wentzcovitch, R. M., J. L. Martins, and G. D. Price (1993), Ab initio molecular dynamics with variable cell shape: application to $MgSiO_3$, *Phys. Rev. Lett.*, *70*, 3947.

Wentzcovitch, R. M., J. F. Justo, Z. Wu, C. R. S da Silva, A. Yuen, and D. Kohlstedtd (2009), Anomalous compressibility of ferropericlase throughout the iron spin cross-over, *Proc. Natl. Acad. Sci.* , *106*, 21.

Wu, Z., J. F. Justo, C. R. S. da Silva, S. de Gironcoli, and R. M. Wentzcovitch (2009), Anomalous thermodynamic properties in ferropericlase throughout its spin crossover, *Phys. Rev. B*, *80*, 014409.

Wu, Z., J. F. Justo, and R. M. Wentzcovitch (2013), Elastic Anomalies in a Spin-Crossover System: Ferropericlase at Lower Mantle Conditions, *Phys. Rev. Lett.*, *110*, 228501.

Wu, Z., and R. M. Wentzcovitch (2014), Spin crossover in ferropericlase and velocity heterogeneities in the lower mantle, *Proc. Natl. Acad. Sci.*, *111(29)*, 10468–10472.

Xu S., S-H. Shim, and D. Morgan (2015), Origin of Fe^{3+} in Fe-containing, Al-free mantle silicate perovskite, *Earth Planet. Sci. Lett.*, *409*, 319-328.